РЕНТГЕНОЛОГИЯ РАДИОЛОГИЯ
ROENTGENOLOGIA RADIOLOGIA

ISSN 0486-400X

2018
Книжка / Number 1
Том / Volume LVII

ПРАВОПРИЕМНИК НА „ИЗВЕСТИЯ НА БЪЛГАРСКОТО РЕНТГЕНОЛОГИЧНО ДРУЖЕСТВО“

Indexed by
Scopus®
Source record id 53718
EMBASE/Excerpta Medica
International Nuclear Information System (INIS)
Bulgarian Citation Index

СПИСАНИЕ НА БЪЛГАРСКАТА АСОЦИАЦИЯ ПО РАДИОЛОГИЯ

JOURNAL OF THE BULGARIAN ASSOCIATION OF RADIOLOGY

РЕНТГЕНОЛОГИЯ
РАДИОЛОГИЯ
PROENTGENOLOGIA
RADIOLOGIA

2018
Книжка / Number 1
Том / Volume LVII

СЪДЪРЖАНИЕ		CONTENTS

АДРЕС ЗА КОРЕСПОНДЕНЦИЯ:
Акад. проф. Светлана Соловьова
solovevasn@yandex.ru

Анализатор на патологията на човешките тъкани – нов инструмент за анализ на компютъртомографските и магнитнорезонансни изображения

Соловьова С. Н.[1], Лешинкова А. В.[1], Урозова В. С.[2], Маткин А. Е.[2], Заболотних Д. В.[1]

[1]Научно-изследователски център „Авантренд“
[2]Урал Федерален университет – Русия, Екатеринбург

ADDRESS FOR CORRESPONDENCE:
Acad. Prof. Svetlana Soloveva
solovevasn@yandex.ru

Pathology analyzer of human tissues – new tool for analysis of CT and MRI images

S. N. Solovieva[1], A.V. Leshinkova[1], V. S. Urosova[2], A. E. Matkin[2], D. V. Zabolotnykh[1]

[1]Scientific and Research Center „Avantrend“
[2]Ural Federal University – Russia, Ekaterinburg

Резюме. Разработеният „Анализатор на патологиите на човешките тъкани“ има за цел да се увеличат диагностичните възможности на стандартните методи за изследване на увреждания на органи и тъкани. Подобряването на диагностичните способности е постигнато чрез въвеждане на нови критерии за количествено оценяване и формализиране на диагностичните характеристики, като структура и тъкан на плътност. Анализаторът на патологията е модулна система, чиито модули са насочени към решаване на специфична задача за подобряване на изображението, оценка на новите критерии и получаване на допълнителна диагностична информация. Настоящата работа обсъжда разработените модули, по-специално системата за подкрепа на диференциалнодиагностичните решения, която позволява да се решат следните задачи: а) изучаване на границите на патологията, например – автоматично определяне на границите на глиома на човешкия мозък (комбиниран метод за обработка на CT и MRI изображения); б) изследване на структурата на туморите и други патологични промени с нови подходи в анализа на медицинските изображения; в) анализ на магнитнорезонансни изображения, използващи стойности, нормализирани към скалата на Hounsfield. Разработени са математически модели за всяка подсистема. Оценката на резултатите от изследванията е извършена съвместно с медицински специалисти от различен профил: рентгенолози, пулмолози; неврохирурзи.

Ключови думи: АНАЛИЗАТОР НА ПАТОЛОГИЧНИ ПРОМЕНИ В ЧОВЕШКА ТЪКАН. ИНСТРУМЕНТ ЗА АНАЛИЗ НА ИЗОБРАЖЕНИЯ. КТ. МР

Abstract. The “Analyzer of human tissue pathologies“ is developed to increase the diagnostic capabilities of standard methods of investigation of organ and tissue damage. Improvement of diagnostic capabilities are achieved by introducing new criterions of quantitative valuation and formalization of diagnostic features, such as structure and tissue of density. The pathology analyzer is a modular system, each module of which is aimed at solving a specific task of image improvement, its evaluation according to new criteria and obtaining additional diagnostic information. The article discusses the developed modules, in particular, the differential diagnostic decision support system, which allows to solve the following tasks: a) assessment the borders of pathologic area. – for example - automatic determination of boundaries of human brain glioma (Combined method of processing CT and MRI images); b) studying the structure of tumors and other pathological changes by creating new approaches in medical images analysis; c) Analysis of MRI images using values normalized by the Hounsfield scale. Mathematical models for each subsystem are developed. Relevance assessment and approbation of the research results is performed with medical experts of different profile: radiologists, pulmonologists, neurosurgeons.

Key words: PATHOLOGY ANALYZER OF HUMAN TISSUE. IMAGE ANALYSIS TOOL. CT. MRI

Introduction

The introduction of computed tomography and the magnetic resonance imaging come out on new diagnotic level. Despite the constant improvement of methods, the challenges of accuracy of visualization, adequate interpretation and valuation remain relevant. So, for example, in 2016 research was conducted on the challenge of a large false-positive factor in the cluster approach of fMRI analysis, and the results of about 40 000 fMRI analyzes were questioned. Consequently, both constant work on new research methods, as well as retrospective analysis, and the development of new approaches to the existing methods and methods for their evaluation are going on.

The data about the internal structure of subject are represented as a DICOM format image. This digital image in computer interpretation is a matrix, and the element located at the intersection of its row and column is called the pixel [17]. Disadvantages of the DICOM – image are occurrence of noise, averaging the values in pixels located on the boundary of two regions [8]. The above listed disadvantages lead to a difficulty in recognizing the pathology of the tissue on the images. All this leads to the fact that working with digital medical images is a complex and time-consuming process.

Evaluation is carried out by visual analysis of images by a radiologist. To simplify the work of a doctor, there is a range of commercially available or free software products. They consist of some amount of modules displaying and navigating images, working with multidimensional medical images. Some are intended only for image visualization. Others, in addition to the basic functions, allow analysis and measurements. Similar universal systems have some limitations. They are not able to take into account the specific features of organs, tissues and particular pathological cases for visualization, and as a consequence for image analysis.

The purpose for developing „Analyzer of human tissue pathologies“ is to enhance the diagnostic capabilities of standard methods of examination of organ and tissue damage, by:

- improving the analysis of the structure of the tumor and other pathological areas on different digital medical images;
- improving the analysis of tumors and pathological areas borders on different digital medical images;
- quantifying pathological changes in different digital medical images;
- identifying the quantitative dependence between CT and MRI imaging when jointly used.

New criteria of quantitative evaluation and formalization of diagnostic features, such tissue structure and density are introduced.

The pathology analyzer is a modular system, each module of which is aimed to respond to a specific task of image improvement, according to new criteria and obtaining additional diagnostic information.

Decision supporting system (DSS) in determinaton the pathology nature in the region of interest

The DSS is an automated computer system helping the operator to analyze and report difficult imaging findings.

Randomly or poorly structured medical diagnostic information in traditional sources, could create difficulties.

The DSS tries to minimize efforts in the analysis of information on the nature of the pathology in the region of interest by processing MRI and CT images. The following tasks are intended:

- analysis of the training sample of various features of pathologies on the basis of machine learning algorithms;
- expert evaluation of an arbitrary set of features based on the obtained algorithms of machine learning;
- restoration of missing features;
- explanation of the process of obtaining the final result.

The decision supporting system concerning the character of the pathology in the region of interest is one of the modules of the tool, working with different areas of interest. Here is an example of the work of the system, considering the lungs as an region of interest:

A sample group of 96 patients was used to train the system. Each patient is characterized by quantitative, nominal and resultant characteristics, examples of which are given in Figures 1 to 3. The total number of symptoms was depending on the values of the analyzed features, each of the patients belonged to one of 5 groups:

- cancer;
- innocent appearance;
- sarcoidosis;
- tuberculosis;
- pulmonary fibrosis.

Глюкоза крови(ммоль/л)

Тип признака: Количественный (float64)

Краткая статистика

	count	mean	std	min	25%	50%	75%	max
Глюкоза крови(ммоль/л)	70	5.52843	0.954649	3.9	5	5.5	6	9.7

Fig. 1. *An example of a quantitative features*

Форма контура образования

Тип признака: Номинальный (float64)

Краткая статистика

	count	mean	std	min	25%	50%	75%	max
Форма контура образования	88	2.64773	1.11458	1	2	2	4	5

Уникальные значения

Значение	Количество
1	12
2	38
3	8
4	29
5	1

Расшифровка значений

Значение	Расшифровка
1	Ровный
2	Бугристый
3	Фестончатый
4	Лучистый
5	Звездчатый

Fig. 2. *An example of a nominal features*

Гистология(итог)

Тип признака: Номинальный (object)

Краткая статистика

	count	unique	top	freq
Гистология(итог)	22	15	умереннодифференцированная аденокарцинома	3

Уникальные значения и их расшифровка

Значение	Количество	Расшифровка
аденокарцинома смешаного типа	1	Здесь должна быть расшифровка значения
гамартома	1	Здесь должна быть расшифровка значения
мелкоклеточная карцинома	2	Здесь должна быть расшифровка значения
нейроэндокринная карцинома низкой дифференцировки	1	Здесь должна быть расшифровка значения
немелкоклеточная карцинома	1	Здесь должна быть расшифровка значения
немелкоклеточная низкодифференцированная карцинома	1	Здесь должна быть расшифровка значения
нет верификации	2	Здесь должна быть расшифровка значения
низкодифференцированная аденокарцинома	2	Здесь должна быть расшифровка значения
низкодифференцированная плоскоклеточная карцинома	1	Здесь должна быть расшифровка значения
отграниченный фокус абсцедирующей пневмонии	1	Здесь должна быть расшифровка значения
плоскоклеточная карцинома низкой дифференцировки	1	Здесь должна быть расшифровка значения
светлоклеточная карцинома	1	Здесь должна быть расшифровка значения
слизеобразующая аденокарцинома	1	Здесь должна быть расшифровка значения
умереннодифференцированная	3	Здесь должна быть

Fig. 3. *Example of the resulting features*

The machine learning algorithms are Decision Tree, Random Forest. The accuracy is estimated using the SVM method [19].

The considered part of the developed decision supporting system defines t to which of the 5 groups of lung pathologies a patient belongs according the set of features.

Assessment of borderlines of pathology area by automatic detection of cerebral glioma borders, based on MRI and CT imaging

The development of the model is related to diagnostic problems in imaging of oncological diseases. The structural complexity of tumors, the limitations of some modern methods in the image formation, processing and analyzing limits the planning of the surgical tumor removal.

A shortage of primary information, backed up by visualization, reduces the possibility of total resection of tumors, which can lead to their recurrence. An analysis model is developed taking into account the structural features of brain gliomas.

The input data are CT and MRI digital images, generated as discribed by Гонсалес Р. Вудс, Р [17]. Upon the problem to solve, under the digital image we mean a matrix of the size M x N of the form:

$$f(x,y)=\begin{bmatrix} f(0,0) & f(0,1) & \cdots & f(0,N-1) \\ f(1,0) & f(1,1) & \cdots & f(1,N-1) \\ \cdot & \cdot & & \cdot \\ \cdot & \cdot & & \cdot \\ \cdot & \cdot & & \cdot \\ f(M-1,0) & f(M-1,1) & \cdots & f(M-1,N-1) \end{bmatrix}. \quad (1)$$

The right side of this equality is by definition a ***digital image.*** Each element of the matrix is called a ***pixel***.

The initial stages of image processing is its correction, by applying various masks, filters, linear transformations, etc., discribed by Гонсалес Р. Вудс, Р [17]. As the input data are CT, MRI images, the choice of the initial stages of image processing is based on the properties of the type of images [18], namely:

- images have low resolution and high degree of noisiness;
- the „partial volume“ effect complicates the exact determination the borderlines.

Property of correlation of signal to noise is governed by formula

$$SN\,C=\frac{S}{\delta}\,, \quad (2)$$

where S – average signal value; δ – standard deviation of background signal.

Consequently, the following stages of preliminary image processing were selected.

Background removal

The average value of the non-uniform background $\hat{n}$ the image L, is calculated, since it is assumed that the image of interest is located in the center of the frame

$$\hat{n}=L^{-1}\sum_{i-1}^{L} n_i\,, \quad (3)$$

where n_i- the value of the background in the i-th element of the resolution along the perimeter of the image.

The summation in (3) occurs only along the perimeter of the rectangular image. Next, the evaluation of the filtered image is formed according to the following rule

$$J_k=\{J_{k-1}-\hat{n}_{k-1}, \text{при } J_{k-1}>\hat{n}_{k-1}\ 0, \text{при } J_{k-1}<\hat{n}_{k-1} \quad (4)$$

When applying this filter two or three times to an image, almost the entire additive background is eliminated.

Increase definition

The processed mage by the formulas (3), (4), undergoes the Fourier transformation [17] and the transition to the spatial frequency domain F $(\vec{w})$. Than, an increase in high spatial frequencies is made, by raising the obtained spectrum to a power whose exponent α is in the range. (0 … 1). This the procedure can be written as follows:

$$F_{k+1}(\vec{w})=[F_{k+1}(\vec{w})]^{\alpha}. \quad (5)$$

Then the inverse Fourier transform of $F_{k+1}(\vec{w})$ and an image with clearly defined details is obtained.

Wiener filter

Wiener filters amplify the intensity of the signal from detected focal changes, which permits to increase the accuracy of segmentation of pathological changes. This method is less susceptible to interference. Information on the spectral densities of image power and noise is used.

Spectral density of signal is governed by correlation

$$S_{II}(v) = F[R(\omega)], \quad (6)$$

where $R(\omega) = \int I(x)I(x-\omega)dx$ – autocorrelation function.

Relative spectral density of signal is governed by correlation

$$S_{II'}(v) = F[R(\omega)], \quad (7)$$

where $R(\omega) = \int I(x)I'(x-\omega)dx$ – cross-correlation.

In the construction of Wiener filter, the task is to minimize the standard deviation of the processed image from the object

$$E\{[I(x,y) - I'(x,y)]^2\} = min, \quad (8)$$

where $E\{\}$ – expectation function.

By converting these expressions, it can be shown that the minimum is reached when the transfer function is determined by the following expression

$$D(v_x, v_y) = \frac{S_{II'}(v_x,v_y)}{S_{II}(v_x,v_y)}. \quad (9)$$

If there isn't noise on the image, then spectral density of noise function is 0 and Wiener filter turns into a normal reverse filter.

At this step, the original image acquires an improved visual representation, while its processing is automatic and with minimal loss of information about the original image.

The next stages are image segmentation and fractal analysis, reflecting the main specificity of the model being developed.

The formal presentation of solved at this stage of the subtasks.

Designations:

a	array of all pixels of the image;
$A = \{A_i\}$	a subarray of pixels that meet the segmentation criteria
$A' = \{A'_j\}$	a subarray of pixels that meet the criteria for fractal growing regions
$\hat{S}$	segmentation operation over a array A
$\hat{F}$	operation of fractal growth of regions over array of A'
K	array of clusters obtained after the procedure $\hat{S}$
K'	array of region, obtained after the procedure $\hat{F}$ $_i$

The subtask of the segmentation of the original image has the form:

$$\hat{S}(a) = \{K_1(A_1), \ldots, K_i(A_i)\} : \ \forall K_i(A_i)\ satisf\ ies\ Q = \{Q_i\},$$

where Q – array of criteria f or the segmentation method .

The subtask of fractal growing of regions has the form:

$$\hat{F}(K'_i(A'_i)) = \{K'_1(A'_1), \ldots, K'_j(A'_j)\} :$$

$$\forall K'_j(A'_j)\ satisf\ ies\ Q = \{Q_i\} \text{ и } H = \{H_i\},$$

where H – array of criteria for growing a fractal region. Subtask definition of the segmentation error and the memorization of new characteristics of regions that meet the criteria. Formally, represent

$$\{K_i(A_i)\} - \{K'_j(A'_j)\} \neq \varnothing. \quad (10)$$

Then, the segmentation in the first step performs with an error found by estimating the difference between the boundaries of clusters and fractal regions. It is necessary to memorize the new features of H, Q and return to step 1, but already having additional counted feature to perform a new iteration of segmentation.

The described sub-task of the segmentation must be performed automatically, without entering additional conditions and static criteria. In this case, at the output must be a clustered image, each cluster of which stores information about the pixels belonging to it, such as: the intensity of the pixel signal, knowledge about neighboring pixels, the pixels on the boundaries. Clustered image decomposition at this stage is the preparation to fractal growth of regions from the center of mass of automatically defined clusters.

Given the specificity of the proposed solution, we use the algorithm for clustering fuzzy k-means [21]. Fuzzy clustering consists in finding a fuzzy partition of the elements of the investigated set of elements into T fuzzy clusters and the corresponding values of the membership functions. The membership function indicates the degree of certainty that the elements of a certain set belong to a given fuzzy set and must satisfy the condition

$$\mu_A(a_i) \geq 0, \ \forall j \in [1, T], \ \forall a_i \in A,$$

where A – analyzed image.

The data matrix is formed from the attribute value vectors:

$$D = [x^1_1 x^1_2 \ldots x^1_q x^2_1 x^2_2 \ldots x^2_q \ldots \ldots \ldots \ldots x^n_1 x^n_2 \ldots x^n_q]$$

The statement of the problem of fuzzy cluster analysis is formed in this way: on the basis of the initial data D, define a fuzzy partition of the set A into a given number of fuzzy clusters, at which the extremum of some objective function is achieved among all the fuzzy partitions.

Additional conditions are imposed on the membership function normalization:

$$\sum_{j=1}^{T} \mu_{A_i}(a_i) = 1, \ \forall a_i \in A,$$

$$\sum_{j=1}^{T} \mu_{A_i}(a_i) = 1, \ \ \forall i \in [1, \ T],$$

where $T \in N$ – number of clusters, $T > 1$, - absence of empty clusters.

For each fuzzy cluster, the q-dimensional vectors of the cluster center are introduced

$$c_i = [c^j_1, c^j_2, \ldots, c^j_q], \ \forall j \in [1, T],$$

each component of which is determined in accordance with the equation:

$$c^j_l = \frac{\sum_i [\mu_{A_j}(a_i)]^m x^j_l}{\sum_i [\mu_{A_j i}]^m} \text{ за } \forall j \in \{1 \ldots T\}, \forall p_l \in P, \quad (11)$$

where m – exponential weight.

The objective function is sum of squares of the weighted deviations of the coordinates of the clustering objects from the centers of the desired fuzzy clusters:

$$\varepsilon(A_j c^j_l) = \sum_{i=1}^{n} \sum_{j=1}^{T} [\mu_{A_j}(a_i)]^m \sum_{l=1}^{q} (x^i_l - c^j_l)^2 . \quad (12)$$

The task of an indistinct clustering is to find the matrix U function values of accessory of a clustering objects to indistinct clusters, that providing a minimum of target function (12).

The specificity of the proposed solution is to use the fractal cluster estimation model to reduce the segmentation error. In this case, it is necessary for each cluster obtained to determine the characteristics of the local fractal model, to grow the region from the center of the cluster, taking into account new features, to estimate the degree of divergence of the cluster and region boundaries, and to conduct the repeated segmentation taking into account new information about the texture.

In Zhuang and Meng, Q. paper [15], an algorithm for image segmentation using fractal dimension is proposed, using wavelet-decomposition coefficients. This method uses a feature vector composed of fractal dimension estimation in 3 directions (horizontal, diagonal and vertical) and several levels (1-3) of wavelet decomposition. Since we are working with discrete signals, there are a finite number of scale values on which it is possible to calculate the estimate of the fractal dimension. Thus, the sequence of values obtained at different resolution levels and orientations is used as a feature vector for the image region under study.

For each element of the image (cluster), the following formula was used

$$D_{\theta,v}(p) = \frac{log\{\sum_{u \in W_{\theta,v}[N(p)]} |u| \sqrt{2^{-v}}\}}{log(v^2)} = \quad (13)$$

$$= \frac{log\{\sum_{u \in W_{\theta,v}[N(p)]} |u| \sqrt{2^{-v}}\}}{v * C},$$

where $N(p) \in K$ - image window, surrounding pixel p inside the cluster, representing the function, for which the fractal dimension is calculated; $v \in \{0,...,log_2 m\}$ - levels of decomposition (resolution) of the discrete wavelet transformation of the cluster, $\theta \in$ [horizontal, vertical, diagonal]; $W_{\theta,v}$ -wavelet - image coefficients; $C = \log 2$ - constant.

The estimation of the fractal dimension, calculated by formula (13) in this article using the wavelet transform, is used to form a multidimensional array of characteristics.

The growth of fractal regions occurs in the same way as described above for the cluster analysis algorithm, taking into account the addition of new characteristics to the matrix

$$D = [x^1_1 x^1_2 \ldots x^1_q x^2_1 x^2_2 \ldots x^2_q \ldots \ldots \ldots \ldots x^n_1 x^n_2 \ldots x^n_q]$$

The evaluation of the areas is obtained using the histograms of the clusters and regions obtained. If

the same element is the cluster, but its fractal dimension, differs from the elements of the region, then it is necessary to take this difference into account. The procedure is repeated for each element. An array of new features of the elements is formed.

At the last iteration of the proposed algorithm, we get a final set of clusters and calculated fractal sizes for each cluster.

Having constructed a histogram of the final processed and analyzed image, the cluster describing the region of glioma is defined as part of a histogram with an uncharacteristic fractal distribution.

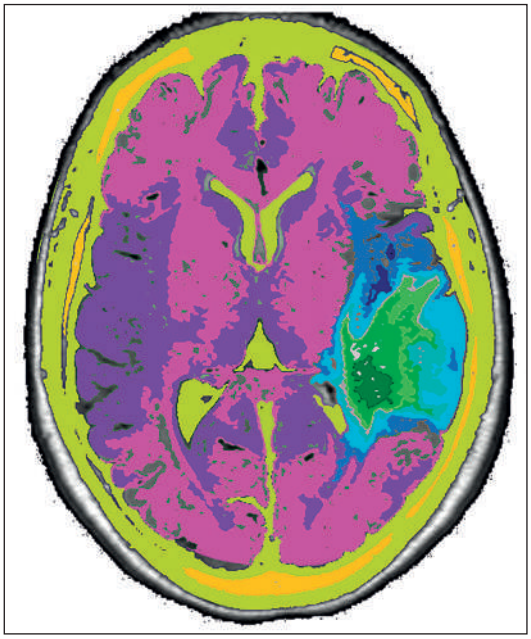

Fig. 4. *Segmentation*

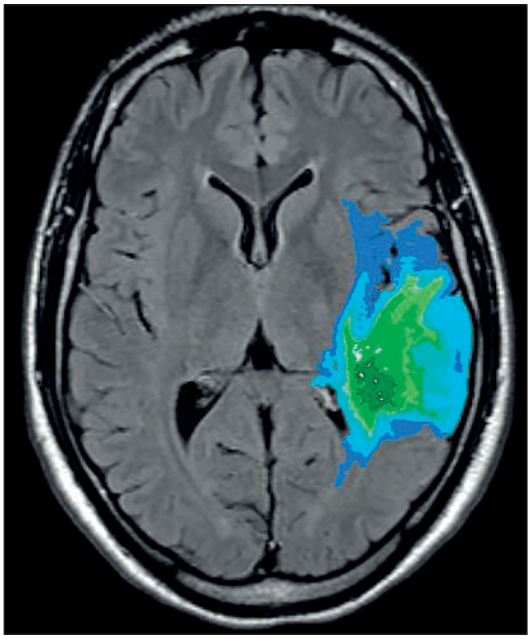

Fig. 5. *Glioma area separate from background*

New approaches in the analysis of digital chest roentgenogram

The radiogram is widely used as first method to detect thorax lesions. It is used as well in screening population. Efficient detection of pathology by chest radiogram is essential. Some technical disadvantages allow visualization limitations.

The purpose of the study is to improve the quality of the analysis, by introduction of new metrics for assessment medical X-ray image, as well a model independent from nosology. In the model, the new metrics, is: value of fractal dimensionality of Minkowski and structural characteristics of the revealed classes of organs, tissues and their sets.

Initially the image is dividedinto clusters by SLIC superpixels method on a texture.

$$A = (a_{11} \dots a_{1n} \vdots \ddots \vdots a_{m1} \dots a_{mn}), \quad (14)$$

where A - source image,

a_{ij} – value of the source image pixels intensity

$$B = (b_1 b_2 \vdots b_k), \quad (15)$$

where B- set of clusters,

b_i – cluster of the textural objects received after splitting, k – quantity of clusters partition.

$$b = (q_1, q_2, q_3, \dots q_l), \quad (16)$$

where q – element of cluster; l – quantity of cluster elements.

For the appeal to cluster elements, it is necessary to make their numbering. On all objects of one cluster, comparing of objects in parameters of a texture and distribution of intensity is executed. One of the simplest approaches applied to the description of a texture consists in use of the statistical characteristics determined by the histogram of intensity of all image or its area.

If the differences of the histogram of intensity and textural characteristics are above a maximum permissible norm, therefore, they are critical and the image has pathological sections.

For calculation of Minkowski fractal dimensionality the following next steps are observed:

- object is covered by a square grid with cells of the known size;
- the quantity of cells in a fragment of the researched object is counted;

- couple of values “size (side length) of a cell“ – “quantity of the cells containing an object“ remain;
- a grid is detailed - i.e. the size of cells decreases, and, respectively, the quantity of the cells containing an object increases;
- a new couple of values remains;
- the procedure of detailing repeats;
- according to a method of computation of dimensionality of Minkowski, its value will be equal to slope of the regression line constructed on the plane on rows of log (N) and log(1/e) values and is calculated on a formula (17)

$$D = \lim_{\varepsilon \to 0} \frac{\ln(N_\varepsilon)}{\ln\frac{1}{\varepsilon}}, \quad (17)$$

where N_ε - the minimum number of sets with diameter ε, which can cover the initial set [16].

- after calculation comparing with critical is executed.

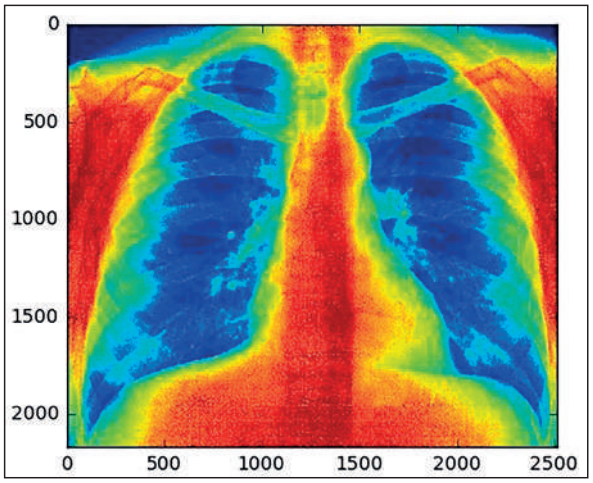

Fig. 6. *Image filtering*

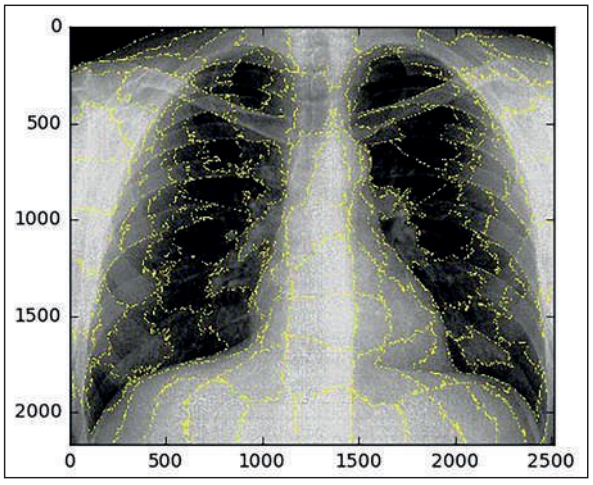

Fig. 7. *Application of the Slic Superpixel classifier*

A method for analyzing MRI images based on values normalized by the Hounsfield scale was developed as well for quantitative evaluation of MRI images and binding to the intensity scale. Such a scale MRI images, then it was created artificially, based on the Hounsfield scale.

The evaluation of the MRI image is based on the signal intensity and aimed at separating the anatomical structures from the difference in contrast, including the detection of abnormalities by the increased or decreased signal value of the study region. In the MRI image, the brightness of each pixel is proportional to the measured MR signal.

The resulting brightness (intensity) is relative and depends on the chosen pulse sequence and capture times. Therefore, the intensity values from one tissue differ from study to study. The intensity of the zone of interest in MRI and CT was assessed collectively, classified, and then the regression problem was solved.

Since the intensity values in the MRI images vary, with different protocol settings, it is necessary to present the MRI intensity values of the image in a set of characteristics by calculating for each pixel the intensity I_i^* in fractions relative to the average intensity obtained from the fat in this image:

$$I_i^* = (-100) * \frac{I_i - I_{fat}}{I_{fat}} \quad (18)$$

Values of I_i^* are the same for tissues of the same nature on different T2-weighted MRI images, i.e. obtained at different capture times and magnetic field forces.

Comparing together the values of the Hounsfield scale on the CT images and the intensity of the MRI images in each region, a set of pairs of values (x, y) were obtained, where x is the image I_i^* MRI value and y is the corresponding CT value, for further calculation of the regression in according to the selected analog.

To describe the complex forms of the distributions of the resulting pairs of values, we use the equation of the generating model of mixture distribution [16]:

$$p(x, y) = \sum_{k=1}^{K} w_k p_k(x, y; \theta_k), \quad (19)$$

where $p_k(x, y; \theta_k)$ – likelihood function of the k-th component;

w_k – eight of the k-th component of the model;

θ_k – vector of distribution parameters.

Parameter $\theta_k = (\mu_k, \sum_k)$, where μ_k – expected value, $\sum_k$ – covariancematrix. Using a mixture of distribution will allow us to describe complex forms of distribution of pairs of values. As a function of the distribution density, the Gaussian distribution function (20) is used in the mixture model, and the mixture model is called the Gaussian mixture.

$$p(x,y) = \frac{1}{2\pi\sigma_x\sigma_y\sqrt{1-\rho^2}} e^{\left(\frac{1}{2(1-\rho^2)}\left(\frac{(x-\mu x)^2}{\sigma_x^2} - \frac{2(x-\mu x)(y-\mu y)}{\sigma x \sigma y} + \frac{(y-\mu y)^2}{\sigma_y^2}\right)\right)}, \quad (20)$$

where $\rho = \frac{\sigma xy}{\sigma_x \sigma_y}$ – correlation coefficient.

When the mixture is separated, the parameters θ and w are selected, so as to achieve the maximum likelihood function. To estimate the parameters, we use the EM algorithm [9], consisting of two stages:

1 parameter estimation:

$$g_{ij} = \frac{w_j p_j(\bar{x}i;\theta_j)}{\sum_{k=1}^{K} w_k p_k(\bar{x}i;\theta_k)}, \quad (21)$$

where xi – the $i\text{-}th$ vector of values (x, y) in the sample,
$i = 1,..,m$ – vector number in the sample,
$j = 1,..,K$ – mixture component number. 2 selection of parameters:

$$\theta_j = arg\ max_\theta \sum_{i=1}^{m} g_{ij} ln\ p_j(\bar{x}_i;\theta) \quad (22)$$

$$w_j = \frac{1}{m}\sum_{i=1}^{m} g_{ij} \quad (23)$$

After evaluating the parameters for given pairs of values, equation (8) can be used for regression. For this, we represent the two-dimensional density distribution function as the product of the conditional density y and the density x and express the conditional density y:

$$p(x) = \frac{p(x,y)}{p(x)} = \frac{\sum_{k=1}^{K} w_k p_k(x,y,\theta_k)}{\sum_{k=1}^{K} w_k p_k(x,\theta_k)} \quad (24)$$

Equation (13) in the following view:

$$p(x) = \sum_{k=1}^{K} w_k(x) p_k(y), \quad (25)$$

where

$$w_k(x) = \frac{w_k p_k(x)}{\sum_{i=1}^{K} w_i p_i(x,\theta_i)} \quad (26)$$

The assumed value in units of the Hounsfield scale from the given value of the MRI intensity can be obtained as a conditional mean:

$$\hat{y} = f(x) = \sum_{k=1}^{K} w_k(x)\bar{\mu}_k(x), \quad (27)$$

where

$$\bar{\mu}(x) = \mu_y + \sum_{YX}\sum_{XX}^{-1}(x - \mu_x) \quad (28)$$

Thus, using the Gaussian mixture, the values of the covariance matrix and the probability weight were obtained, for the initial data set. Using them in equation (13), we get the value of the Hounsfield scale for a given x (the value of the MRI intensity).

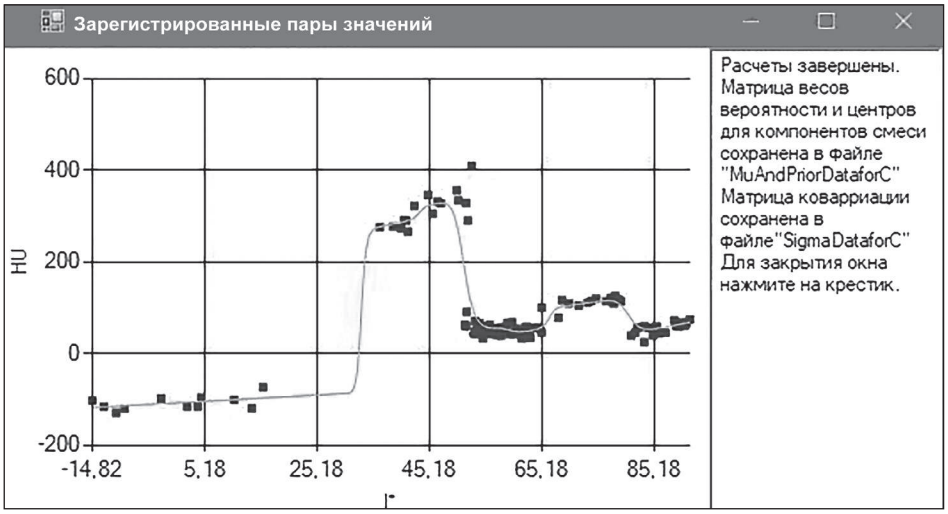

Fig. 8. *Regression of values*

Color mapping is one of the methods that function in a program for processing medical images.

To solve the problems of visualization and analysis of the structural features of the tissues of individual organs and areas of interest, the color map method, which does not have a binding to the original „windows“ was used.

This palette was obtained by us through analytical and experimental studies aimed at detecting densitometric indicators of various organs and tissues..

The analytical study was carried out on the basis of scientific works devoted to the review of pathologies of various organs, tissues and structures. These works included a densitometric analysis of areas of interest in the normal and pathological state.

Thus, information on the ranges of density values in Hounsfield units was accumulated and analyzed.

In the study, a number of studies were analyzed and mean values (HU) were revealed for a number of anatomical structures [1-5, 7, 10, 12-14]. The results for the 3 areas of interest are shown in Tabl. 1:

Tabl. 1.

ROI	Mean (HU)	SD	Mean (SD)
Lungs	- 861,706	47,94909	50,552
Liver	53,4333	7,309811	18,075
Kidneys	33,39091	13,2665	8,66667

Then, an experimental study was performed during which the areas of interest of CT studies (n = 32) provided by various medical institutions were analyzed and evaluated. The measurements were taken from images of different quality of various CT devices that lack hardware artifacts and areas of increased contrast (distortion due to high-density objects, such as metal structures) in freely distributed 3DSlicer software. The results for the 3 areas of interest are shown in Tabl. 2.

Tabl. 2

ROI	Значение (HU)	SD	Mean(SD)
Lungs	- 853,1	39,25851	76,08
Liver	59,124	6,779891	24,1394
Kidneys	39,11	42,88443	32,5875

The resulting samples of mean values were analyzed for similarity. As a result of the analysis, the characteristics of the samples compared to the mean values coincide at the significance level $p < 0.05$. In this case, the samples consisting of the root-mean-square deviations coincide only with the significance level $p < 0.1$.

The results of the comparison suggest that there is no significant similarity between the values obtained analytically and experimentally. In this case, the data obtained by experimental means are homogeneous, and the sample has a normal distribution.

Based on the experimental data obtained in a single methodology, an information system for the automated analysis of pathological changes was developed. X-ray density values were used to obtain a color map. Each grayscale pixel was assigned a color value (RGB), based on the generated color map. The goal was not just the coloring of the anatomical structure, but the use of color in order to emphasize the gradients between healthy and affected tissue. Thus, for each zone of interest, it became possible to obtain a quasi-histological visualization taking into account healthy/diseased tissue.

An example of the program‘s work on the „Liver“ area of interest is shown in the figures 9 –10.

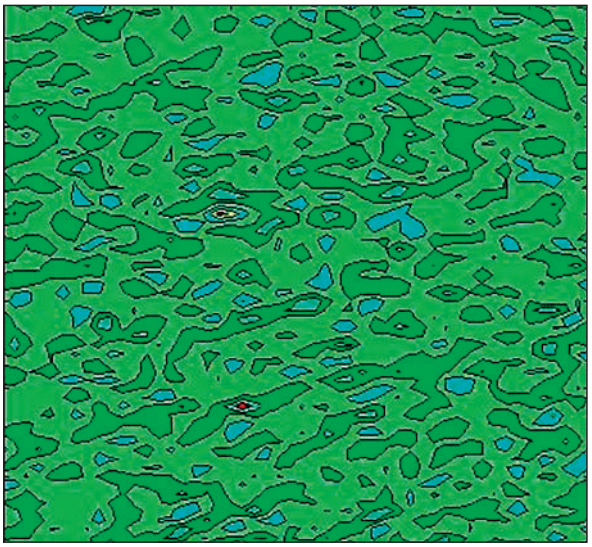

Fig. 9. *Healthy liver tissue*

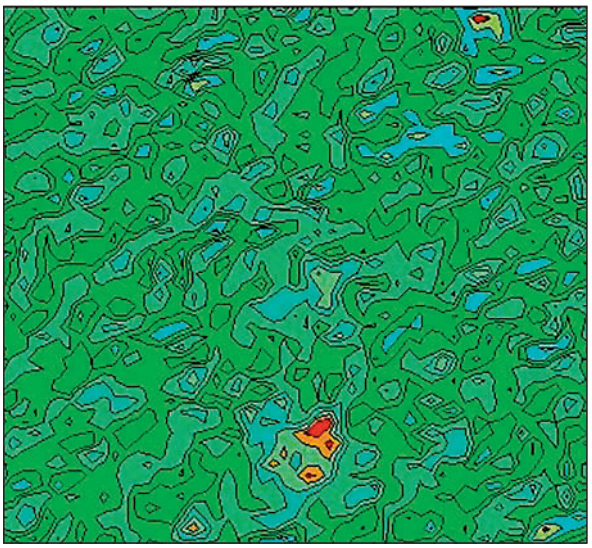

Fig. 10. *Diseasedliver tissue*

Thus, a new tool in interpreting data obtained from digital medical images is proposed. The , investigation was performed together with medical experts of different profile: radiologists, pulmonologists; neurosurgeons.

At this stage, the tool „Pathology analyzer of human tissues“ has many potentials for the development and optimizing of existing subsystems and the creation of new ones to cover other areas of medical imaging.

References

1. *Alomari, R. S., Kompalli, S., Chaudhary, V*. Segmentation of the liver from abdominal CT using Markov random field model and GVF snakes. In Complex, Intelligent and Software Intensive Systems. CISIS 2008:293-8.
2. *Barrett, T., Bowden, D. J., Shaida, N., Godfrey, E. M., Taylor, A., Lomas, D. J., Shaw, A. S.* Virtual unenhanced second generation dual-source CT of the liver: is it time to discard the conventional unenhanced phase?. European journal of radiology. 2012;81:1438-45.
3. *Bellin, M. F., Renard-Penna, R., Conort, P., Bissery, A., Meric, J. B., Daudon, M., et al*. Helical CT evaluation of the chemical composition of urinary tract calculi with a discriminant analysis of CT-attenuation values and density. European radiology. 2004;14(11):2134-40.
4. *Berber, E., Foroutani, A., Garland, A. M., Rogers, S. J., Engle, K. L., Ryan, T. L., Siperstein, A. E*. Use of CT Hounsfield unit density to identify ablated tumor after laparoscopic radiofrequency ablation of hepatic tumorsrid=“‘ id=“‘ Presented at the annual meeting of the Society of American Gastrointestinal Endoscopic Surgeons (SAGES), Atlanta, Georgia, USA. 2000;14:799-804.
5. *De Oliveira, G. A., Del Caro, S. R., Lamego, C. B., Vargas, P. M., Vervloet, V. E. C*. Radiographic plain film and CT findings in lipoid pneumonia in infants following aspiration of mineral oil used in the treatment of partial small bowel obstruction byAscaris lumbricoides. Pediatric radiology. 1985;15:157-160.
6. *Eklunda, A., Nicholsd, T. E., Knutssona, H*. Cluster failure: Why fMRI inferences for spatial extent have inflated false-positive rates. PNAS. 2016:113 - 33.
7. *Graser, A., Johnson, T. R., Chandarana, H., Macari, M*. Dual energy CT: preliminary observations and potential clinical applications in the abdomen. European radiology. 2009;19(1):13.
8. https://habrahabr.ru/post/252429. (accessed March 26, 2015).
9. *Lawrence, C. E., Reilly, A. A.* An expectation maximization (EM) algorithm for the identification and characterization of common sites in unaligned biopolymer sequences. Proteins: Structure, Function, and Bioinformatics. 1990;7:41-51.
10. *Lundquist, H., Hedenstierna, G., Strandberg,* Å**.,** *Tokics, L., Brismar, B.* CT-assessment of dependent lung densities in man during general anaesthesia. Acta Radiologica. 1995;36:626-32.
11. *Mildenberger, P., Eichelberg, M., & Martin, E*. Introduction to the DICOM standard. European radiology. 2002; 2:920-7.
12. *Ouzaid, I., Al-qahtani, S., Dominique, S., Hupertan, V., Fernandez, P., Hermieu, J. F., et al*. A 970 Hounsfield units (HU) threshold of kidney stone density on non-contrast computed tomography (NCCT) improves patients' selection for extracorporeal shockwave lithotripsy (ESWL): evidence from a prospective study. BJU international. 2012.
13. *Schindera, S. T., Nelson, R. C., Mukundan Jr, S., Paulson, E. K., Jaffe, T. A., Miller, C. M., et al*. Hypervascular liver tumors: low tube voltage, high tube current multi–detector row CT for enhanced detection—phantom study. Radiology.2008;246(1):125-132.
14. *Sommer, C. M., Schwarzwaelder, C. B., Stiller, W., Schindera, S. T., Stampfl, U., Bellemann, N., et al.* Lodine removal in intravenous dual-energy CT-cholangiography: Is virtual non-enhanced imaging effective to replace true non-enhanced imaging?. European journal of radiology. 2012;81(4):692-9.
15. *Zhuang, X., Meng, Q.* Local fuzzy fractal dimension and its application in medical image processing. Artificial Intelligence in Medicine. 2004;32:29-36.
16. *Айвазян, С. А., Бухштабер, В. М., Енюков, Е. С.* Прикладная статистика. Классификация и снижение размерности. 1989.
17. *Гонсалес Р. Вудс, Р.* Цифровая обработка изображений. Техносфера. 2005;2:1072.
18. *Магонов, Е. П., Прахова, Л. Н., Ильвес, А. Г., Катаева, Г. В., Трофимова, Т. Н.* Автоматическая сегментация МРТ-изображений головного мозга: методы и программное обеспечение. ВИЧ-инфекция и иммуносупрессиия. 2014;6:737.
19. *Паутов, К. Г., Попов, Ф. А.* Информационная система анализа и тематической классификации веб-страниц на основе методов машинного обучения. Современные проблемы науки и образования. 2012;6:73-7.
20. *Симонян, Г. С., Симонян, А. Г.* Фрактальность биологических систем. III фрактальность органов и организмов. Международный журнал прикладных и фундаментальных исследований. 2016;3:272-6.
21. *Тараскина, А. С.* Нечеткая кластеризация по модифицированному методу с-средних и ее применение для обработки микрочиповых данных. Новосибирск: Проблемы интеллектуализации и качества систем информатики. 2006; 217-228.